Internal Mobility of Reactive-Site-Hydrolyzed Recombinant *Cucurbita maxima* Trypsin Inhibitor-V Characterized by NMR Spectroscopy: Evidence for Differential Stabilization of Newly Formed C- and N-Termini[†,‡]

Jianhua Liu,[§] Om Prakash,[§] Ying Huang,[§] Lisa Wen,[||] Joanna J. Wen,[||] Jeng-Kuen Huang,[||] and Ramaswamy Krishnamoorthi*[,§]

Department of Biochemistry, Kansas State University, Manhattan, Kansas 66506, and Department of Chemistry, Western Illinois University, Macomb, Illinois 61455

Received April 17, 1996; Revised Manuscript Received July 24, 1996[⊗]

ABSTRACT: The solution structure and internal dynamics of the reactive-site (Lys^{44}−Asp^{45} peptide bond) hydrolyzed form of recombinant *Cucurbita maxima* trypsin inhibitor-V (rCMTI-V*) were characterized by the application of two-dimensional ^{1}H−^{15}N NMR methods to the uniformly ^{15}N-labeled protein. The ^{1}H−^{15}N chemical shift correlation spectra of rCMTI-V* were assigned, and the chemical shift data were compared with those available for rCMTI-V [Liu, J., Prakash, O., Cai, M., Gong, Y., Huang, Y., Wen, L., Wen, J. J., Huang, J.-K., & Krishnamoorthi, R. (1996) *Biochemistry 35*, 1516−1524] and CMTI-V* [Cai, M., Gong, Y., Prakash, O., & Krishnamoorthi, R. (1995) *Biochemistry 34*, 12087−12094] for which three-dimensional solution structures have been determined. It was deduced that the solution structure of rCMTI-V* was almost the same as that of CMTI-V*. ^{15}N spin−lattice and spin−spin relaxation rate constants (R_1 and R_2, respectively) and {^{1}H}−^{15}N steady-state heteronuclear Overhauser effects were measured for the peptide NH units and arginine and tryptophan N$_\epsilon$H groups in rCMTI-V*, and the model-free parameters [Lipari, G., & Szabo, A. (1982) *J. Am. Chem. Soc. 104*, 4546−4559, 4559−4570] were computed. Most of the backbone of rCMTI-V* is found to be highly constrained ($\langle S^2 \rangle = 0.85$), including the N-terminal residues 3−6 ($\langle S^2 \rangle = 0.77$). Residues 39−44, forming the C-terminal fragment of the binding loop, exhibit increased mobility ($\langle S^2 \rangle = 0.51$); however, the N-terminal segment (residues 46−48) retains rigidity as in the intact form ($\langle S^2 \rangle = 0.83$). The S^2 values, 0.78 and 0.59, respectively, of Arg^{50} and Arg^{52} side chain NHs provide evidence not only for the conservation of the Arg hydrogen-bonds with the binding loop segments but also for the difference in strength between them. This is consistent with the earlier observation made from a study of rCMTI-V at two different pHs and its R50 and R52 mutants [Cai, M., Huang, Y., Prakash, O., Wen, L., Dunkelbarger, S. P., Huang, J.-K., Liu, J., & Krishnamoorthi, R. (1996) *Biochemistry 35*, 4784−4794]. The dynamical results suggest the main-chain oxygen atom of Asp^{45} as the hydrogen bond acceptor of Arg^{50}. Residues Trp^{9} and Trp^{54}, which interact with many others in the protein scaffold and the binding loop region, respectively, remain rigid in the cleaved inhibitor with the S^2 values of 0.84 and 0.71 determined for their respective N$_\epsilon$Hs. The internal dynamics of rCMTI-V* was compared with that of the noncovalent complex formed between the two fragments of reactive-site-hydrolyzed chymotrypsin inhibitor-2 from barley seeds [CI-2; Shaw, G. L., Davis, B., Keeler, J., & Fersht, A. R. (1995) *Biochemistry 34*, 2225−2233], another potato I family inhibitor that lacks the Cys^{3}−Cys^{48} disulfide present in rCMTI-V*.

Cucurbita maxima trypsin inhibitors (CMTIs[1]) are also potent, specific inhibitors of human blood coagulation factor XIIa (Hojima et al., 1982; Wieczorek et al., 1985; Krishnamoorthi et al., 1990; Wynn & Laskowski, 1990). The potato inhibitor I family member, CMTI-V ($M_r \sim 7$ kDa), has been characterized in considerable detail; its NMR solution structure has been determined (Cai et al., 1995a) to be highly similar to those of two other members of the family for which three-dimensional structures are known: barley chymotrypsin inhibitor-2 (CI-2; McPhalen & James, 1987; Ludvigsen et al., 1991) and eglin c (Hipler et al., 1992; Hyberts et al., 1992). However, in contrast to these inhibitors, CMTI-V possesses a Cys^{3}−Cys^{48} disulfide bridge, and this has been implicated in the reduced mobility of the N-terminal residues in recombinant CMTI-V (rCMTI-V; Liu et al., 1996). The reactive-site (Lys^{44}−Asp^{45} peptide bond)-

[†] This work has been supported by grants from the National Institutes of Health (HL-40789 to R.K. and HL-52235 to L.W.) and the American Heart Association, Kansas Affiliate (KS-95-GS-14 to R.K.). R.K. is supported by an NIH Research Career Development Award (HL-03131). The 11.75 T NMR instrument at KSU was acquired by means of an NSF-EPSCoR grant.

[‡] This is contribution 97-19-J from the Kansas Agricultural Experiment Station.

* To whom correspondence should be addressed. Phone: (913) 532-6262. FAX: (913) 532-7278. E-mail: krish@ksu.ksu.edu.

[§] Kansas State University.

[||] Western Illinois University.

[⊗] Abstract published in *Advance ACS Abstracts,* September 1, 1996.

[1] Abbreviations: CMTI, *Cucurbita maxima* trypsin inhibitor; rCMTI-V, recombinant *C. maxima* trypsin inhibitor-V; CMTI-V*, reactive-site-hydrolyzed *C. maxima* trypsin inhibitor-V; rCMTI-V*, reactive-site-hydrolyzed recombinant *C. maxima* trypsin inhibitor-V; NMR, nuclear magnetic resonance; NOE, nuclear Overhauser effect; HSQC, heteronuclear single-quantum coherence; ppm, parts per million; TOCSY, total correlated spectroscopy; CI-2, chymotrypsin inhibitor-2 from barley seeds; RMSD, root mean-squared deviation; RP-HPLC, reverse-phase high-pressure liquid chromatography.

S0006-2960(96)00932-4 CCC: $12.00 © 1996 American Chemical Society

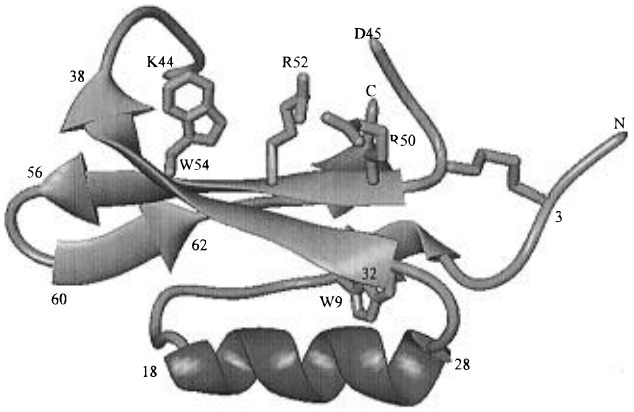

FIGURE 1: Ribbon representation of the three-dimensional solution structure of CMTI-V* (Cai et al., 1995b), showing the side chains of Arg^{50}, Arg^{52}, Trp^{9}, and Trp^{54}. The binding loop fragments retain the hydrogen-bonding interactions provided by the two arginine residues.

hydrolyzed form of CMTI-V (CMTI-V*) suffers a marked reduction in its ability to inhibit both trypsin and factor XIIa (Cai et al., 1995b). The three-dimensional solution structure of CMTI-V* (Figure 1) has been reported, and the thermodynamics of the equilibrium, CMTI-V $\rightleftarrows$ CMTI-V*, has been characterized (Cai et al., 1995b). The clipped inhibitor retains the overall folding and the secondary structure elements of CMTI-V. However, major structural changes occur in the binding loop region. The two fragments of the binding loop, which are connected by the $Cys^{3}-Cys^{48}$ linkage, move apart and display higher root mean-squared deviations (RMSDs), very likely suggestive of increased mobility, in the family of NMR structures generated on the basis of distance and dihedral angle constraints. The binding loop segments are found to retain their hydrogen-bonding interactions with Arg^{50} and Arg^{52} side chains in the rigid core of the protein, as indicated by the stereospecific assignments of the Arg side chain hydrogens (Cai et al., 1995b−d). Very recently, the contributions of Arg^{50} and Arg^{52} to the binding loop flexibility and stability have been characterized (Cai et al., 1996).

In recent years, structural descriptions have become available for intact and cleaved forms of an increasing number of serine proteinase inhibitors of different families in both solid and solution phases; in the case of ovomucoid third domains of the Kazal family (Laskowski & Kato, 1980), X-ray crystal structures (Papamokos et al., 1982; Bode et al., 1985; Musil et al., 1991; Huang et al., 1995) and NMR solution structures (Krezel et al., 1994; Wolkenhorst et al., 1994) have been determined for intact and clipped forms of a few members. Three-dimensional structures have been described for the squash family inhibitor, CMTI-I, in the crystalline (Bode et al., 1989) and solution states (Holak et al., 1989a,b). Secondary structures of CMTI-I* and CMTI-III* have been characterized by NMR (Krishnamoorthi et al., 1992a,b). In the case of eglin c, a potato I family inhibitor, both solid- and solution-phase structures are available (Hipler et al., 1992; Hyberts et al., 1992); in addition, a crystal structure has been described for the reactive-site-hydrolyzed inhibitor (Betzel et al., 1993). In all the aforementioned studies, major structural changes are noted in the binding loop region.

Theoretical studies of protein dynamics (Karplus & McCammon, 1983; Karplus, 1986) have indicated the importance of internal motions in protein function. These motions, occurring on time scales ranging from picoseconds to seconds, are detected by NMR relaxation measurements of ^{13}C and ^{15}N nuclei attached to hydrogens (Peng & Wagner, 1994). It has been pointed out that the precision and accuracy of NMR solution structures of a protein can be improved by using more distance and angular constraints, for example, by accomplishing stereospecific assignments of side chain hydrogens of amino acid residues (Basus, 1989; Clore et al., 1990a,b). Therefore, whenever higher root mean-squared deviation (RMSD) values are encountered, as in the N-terminal region and the clipped binding loop segments of CMTI-V* (Cai et al., 1995b), the question arises as to whether the observed uncertainties are due to insufficient NMR constraints, which is generally the case in unstructured regions, or due to relatively greater flexibility compared to the rest of the protein molecule. In the case of CMTI-V*, we are furthermore interested in characterizing the internal dynamics of Arg^{50} and Arg^{52} side chains to obtain information on the effect of hydrolysis on the relative strengths of the hydrogen bonds made by these residues, information that cannot be obtained from the structural investigation reported (Cai et al., 1995b). Shaw et al. (1995) utilized information from a study of the backbone dynamics of the non covalent complex formed between two fragments of CI-2 to infer structural details.

Herein, we report the determination of dynamical parameters of rCMTI-V* from ^{15}N longitudinal and transverse relaxation rates (R_1 and R_2, respectively) and $\{^1H\}-^{15}N$ heteronuclear Overhauser effects (NOEs). The results demonstrate the difference in internal mobility exhibited by the two fragments of the binding loop. They also suggest probable hydrogen bond acceptors of Arg^{50} and Arg^{52} side chains.

MATERIALS AND METHODS

Protein. Uniformly ^{15}N-labeled rCMTI-V was overexpressed in *Escherichia coli*, isolated, and purified, as described previously (Wen et al., 1993; Liu et al., 1996). The *E. coli* cells were grown in a medium that contained $^{15}NH_4Cl$ as the sole nitrogen source. rCMTI-V* was obtained by reacting rCMTI-V with trypsin (∼5% by mole) and purifying the reaction mixture by reverse-phase high-pressure liquid chromatography (RP-HPLC; Krishnamoorthi et al., 1990). As compared to the native hydrolyzed protein, the recombinant version used in the present study possessed an unacetylated N-terminus that carried an additional Gly residue (Huang et al., unpublished results). The extra N-terminal residue was numbered −1 for the sake of maintaining consistency in numbering between the native and recombinant protein. For NMR studies, a sample of ∼2 mM ^{15}N-labeled rCMTI-V* was prepared by dissolving the lyophilized protein in 0.5 mL of 90% H_2O/10% D_2O (v/v) and adjusting the pH of the solution to 5.4 with 0.2 M HCl and/or 0.2 M KOH.

NMR Spectroscopy. NMR experiments were performed at 30 °C with a 11.75 T (499.496 MHz for ^1H) Varian UNITY*plus* instrument. Two-dimensional HSQC (Bodenhausen & Ruben, 1980; Kay et al., 1989a) and ^{15}N-edited HSQC-TOCSY (Bodenhausen & Ruben, 1980; Cavanagh et al., 1991; Palmer et al., 1991) spectra were recorded with spectral widths of 7000 and 3500 Hz for the ^1H and ^{15}N

dimension, respectively, with 4096 × 256 complex data points in the $f_1(^1H) \times f_2(^{15}N)$ dimensions. A value of 4.71 ppm assigned to the H_2O peak was used as the ^1H chemical shift reference; a value of 380.23 ppm assigned to CH_3NO_2 (Live et al., 1984) served as the ^{15}N chemical shift reference.

Spin−lattice relaxation rate constants (R_1), spin−spin relaxation rate constants (R_2), and $\{^1H\}-^{15}N$ steady-state NOE enhancements were measured for backbone and side chain NH groups in rCMTI-V*, as described earlier (Liu et al., 1996); two-dimensional sensitivity-enhanced pulse sequences (Cavanagh et al., 1991; Palmer et al., 1991) were employed for inversion−recovery (Vold et al., 1968), Carr−Purcell−Meiboom−Gill (CPMG) spin-echo (Meiboom & Gill, 1958), and steady-state NOE (Noggle & Shirmer, 1971) measurements, as described by Skelton et al. (1993). For each measurement, 176 increments of 4K data points each were acquired with 8, 16, and 16 transients per block for R_1, R_2, and NOE experiments, respectively. A total recycling delay of 5 s was used for R_1 and R_2 and NOE measurements. Spectral widths were set to 7000 and 3500 Hz for the ^1H and ^{15}N dimension, respectively. For the R_1 measurements, eight spectra were recorded using relaxation delays of 0.008, 0.05, 0.12, 0.25, 0.4, 0.7, 1.1, and 2.5 s, whereas seven spectra were recorded with relaxation delays of 0.015, 0.032, 0.055, 0.13, 0.23, 0.34, and 0.52 s during the CPMG period for R_2 experiments. NOE measurements were repeated three times. A line-broadening factor of 6 Hz was applied to the f_2 dimension, and a shifted Gaussian window function was applied to the f_1 dimension. A shifted Gaussian window function was applied to both dimensions to resolve the overlap of cross-peaks of Gly^5 and Gly^{59}, Arg^{58} and Leu^{12}, Val^{15} and Arg^{26}, and Cys^3 and Lys^6. The solvent signal was removed digitally prior to Fourier transformation (Marion et al., 1989).

Measurements of ^{15}N Relaxation Parameters and Calculations of Model-Free Parameters. The same procedure described previously for the characterization of backbone dynamics of rCMTI-V (Liu et al., 1996) was followed. The relaxation rate constants were determined by nonlinear least-squares fitting of experimental peak heights to the following equations:

$$I(t) = I_\infty - (I_\infty - I_0)\exp(-R_1{*}t) \quad (1)$$

$$I(t) = I_0 \exp(-R_2 t) \quad (2)$$

where t is the parametical relaxation delay in each measurement, I_∞ is the long-time steady-state resonance intensity, R_1 is the spin−lattice relaxation rate constant, and R_2 is the spin−spin relaxation rate constant. Uncertainties in peak heights were assessed by RMS baseline noise level. Heteronuclear NOEs were calculated by

$$\eta = I_{sat}/I_{unsat} \quad (3)$$

in which I_{sat} and I_{unsat} are the experimental peak heights measured from spectra recorded with and without proton irradiation during the recycling delay, respectively. Uncertainties were calculated by the sum of the RMS of the uncertainties of peak heights about the RMS baseline noise level for I_{sat} and I_{unsat}. Repeated NOE measurements were averaged. The overall correlation time, τ_m, was estimated by a trimmed average of the R_2/R_1 ratios. Model-free parameters (Lipari & Szabo, 1982a,b)−generalized order parameters, S^2, effective internal correlation time, τ_e, and a term to account for chemical exchange and/or conformational averaging, R_{ex}−were calculated, as described previously (Clore et al., 1990b; Palmer et al., 1991; Liu et al., 1996), using the software Model Free (version 3.0) provided by Dr. Arthur G. Palmer, III, of Columbia University, New York.

RESULTS

Assignments of $^1H-^{15}N$ Chemical Shift Correlation Spectra and Structural Characteristics of rCMTI-V.* Advantage was taken of the availability of ^1H and ^{15}N NMR assignments made for rCMTI-V (Liu et al., 1996) and ^1H NMR assignments made for CMTI-V* (Cai et al., 1995b). A comparison of the $^1H-^{15}N$ HSQC spectra of rCMTI-V (Liu et al., 1996) and rCMTI-V* resulted in straightforward assignments of many of the cross-peaks. Those that could not be assigned likewise were assigned by taking into account their coupling patterns in the ^{15}N-edited HSQC-TOCSY map. The assignments were also verified by comparing the ^1H chemical shifts with those of the native CMTI-V* (Cai et al., 1995b). Complete assignments of the $^1H-^{15}N$ HSQC cross-peaks of rCMTI-V* are shown in Figure 2. Backbone ^{15}N NMR chemical shifts of rCMTI-V and rCMTI-V* are compared in Figure S-1 (in supporting information). As expected, the chemical shift changes are mainly confined to the binding loop residues. A comparison of ^1H NMR chemical shifts of backbone NH groups of rCMTI-V* and CMTI-V* (Figure S-2 in supporting information) does not reveal any significant perturbations, except for residue 27, and thus provides evidence that the solution structure of rCMTI-V* is highly similar to that of CMTI-V* whose three-dimensional solution structure has been recently reported (Cai et al., 1995b). In addition, we have also demonstrated that rCMTI-V has the same solution structure as that of native CMTI-V (Liu et al., 1996). Thus, on the basis of these facts, it is reasonable to conclude that rCMTI-V* has the same three-dimensional solution structure as that of CMTI-V* (Figure 1; Cai et al., 1995b), which contains the following secondary structure elements: an α-helix (residues 18−28), three pairs of β-sheets (residues 7−9 and 62−60 antiparallel to residues 67 and 66 and 54−56, respectively, and residues 32−38 parallel to 50−56), and four turns (type II, 12−15; type I, 28−31 and 47−50; and type III, 56−59); the two fragments of the cleaved binding loop (residues 39−44 and 45−49) probably adopt the same conformations in both native and recombinant CMTI-V*.

^{15}N Relaxation Data and Order Parameters. Data sets are expected for 61 backbone ^{15}NHs−excluding those of the N-terminal Gly, Asp^{45} at the cleaved site, and six Pro residues−and eight side chain ^{15}NHs. Relaxation data (R_1, R_2, and NOE; Table S-1 in supporting information) were reliably obtained for 60 backbone and 4 side chain ^{15}NHs and are presented in Figure 3. Cross-peaks for Ser^1 backbone and four of the six Arg side chain ^{15}NHs were not observed. An R_2/R_1 ratio of 2.216 ± 0.151 was used to estimate an overall correlation time, τ_m, of 4.05 ± 0.27 ns. This value of τ_m was used to calculate the Lipari and Szabo parameters (Table S-2 in supporting information) shown in Figure 4. The final, globally optimized τ_m value for rCMTI-V* was 3.93 ± 0.02 ns. The data analysis assumed an overall isotropic tumbling of the protein molecule.

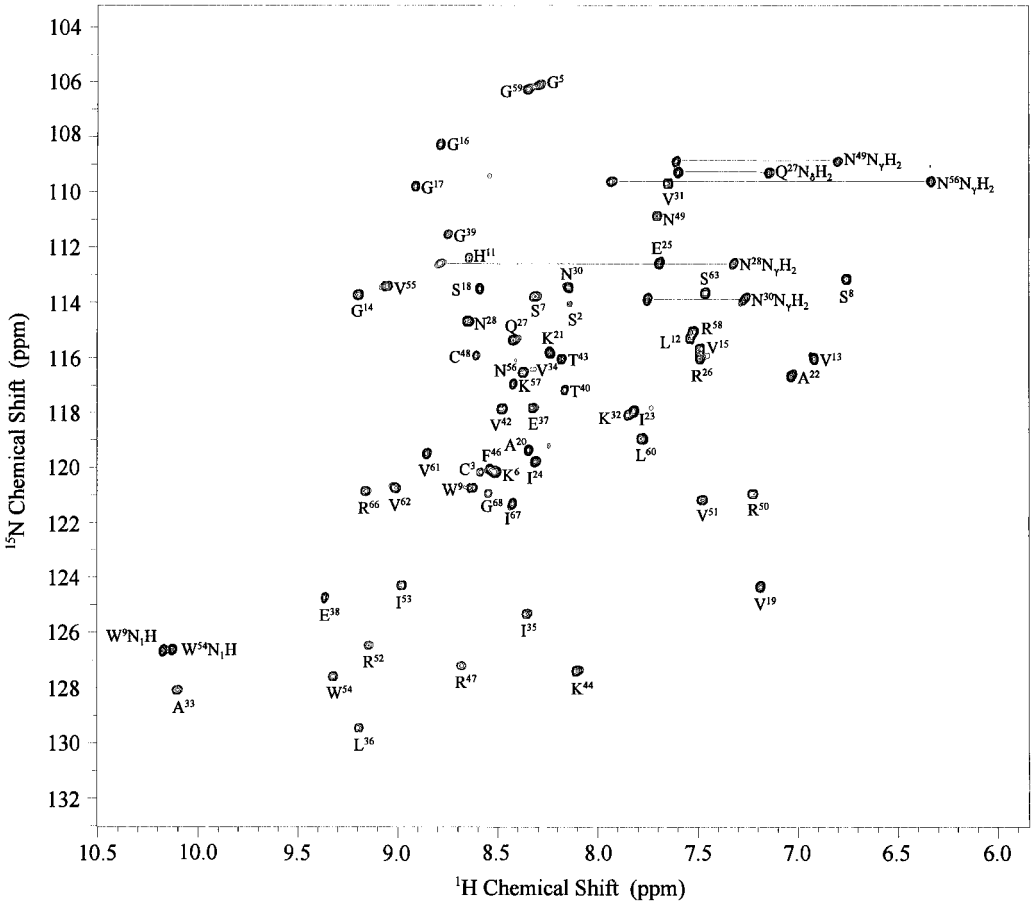

FIGURE 2: ^{1}H−^{15}N HSQC map of rCMTI-V* at 30 °C and pH 5.4, with NH assignments marked by the one-letter name and residue number.

The order parameters calculated for rCMTI-V* (Figure 4A; Table S-2 in supporting information) indicate that its backbone is highly constrained, including the N-terminal region (residues 3−6) and the binding loop fragment made up of residues 46−48. In contrast, the first binding loop fragment (residues 39−44) is highly mobile. The average S^2 values calculated for the α-helix, β-strands, turns, the N-terminal region, and the binding loop fragments are given in Table 1. Of particular interest is the fact that, while the first fragment residues, 39−44, are highly mobile, the second fragment residues, 46−49, are as rigid as those in the structured regions of the protein (Table 2). The effective correlation times, τ_e, of most residues are within 120 ps (Figure 4B). Conformational exchange terms were included for 17 residues, with the highest value being 1.27 Hz (Figure 4C). Side chain N_ϵHs of Arg^{50}, Arg^{52}, Trp^{9}, and Trp^{54} are found to be rigid (Table 3). The N_ϵHs of other arginines (26, 47, 58, and 66) were not observed under the current experimental conditions. The side chains of these arginines were found to be freely mobile in the intact protein (Cai et al., 1996), and that is most likely the case with the hydrolyzed inhibitor.

DISCUSSION

Comparison of the S^2 values of the secondary structure elements between intact and modified rCMTI-V (Figure 4A and Table 1) indicates no significant changes in the rigidity of the helix or the sheet structures. Residues 7, 8, 30, 37, 55, 57, and 63 appear to have slightly increased rigidity in the clipped inhibitor (Figure 4A). The N-terminal rigidity may be ascribed to the Cys^{3}−Cys^{48} disulfide bridge, which pulls the second binding loop fragment (45−48) toward the N-terminal region (Cai et al., 1995b). The β-strand pairs in rCMTI-V* ($\beta_1\beta_6$, $\beta_2\beta_3$, and $\beta_4\beta_5$) show very similar average order parameters. The average order parameter seems to be slightly higher in rCMTI-V* than in rCMTI-V for residues 28−31 in turn II$_a$. The largest R_{ex} values obtained for rCMTI-V* are associated with turn I and turn III (Table S-2), suggesting the presence of motions that occur on a time scale slower than the protein's overall rotational correlation time.

Binding Loop Residues and Side Chains of Arg^{50} and Arg^{52}. The residues forming the reactive-site loop, 39−48, display interesting changes in mobility upon hydrolysis of the Lys^{44}−Asp^{45} peptide bond (Table 2 and Figure 4A). Residues 39−44 show significant decreases in their order parameters, which range from 0.73 to 0.31. These residues forming the new C-terminus of the clipped binding loop are thus very mobile. In contrast, Phe^{46} shows an increased order parameter, from 0.72 ± 0.01 in rCMTI-V to 0.84 ± 0.01 in rCMTI-V*. Similarly, the next three residues (47−49) remain as rigid as they are in the intact protein. This suggests that the strength or stability of the Arg^{50} hydrogen bond (Cai et al., 1995a,b) is unaffected by the peptide bond cleavage. The pH-dependent dynamical study of rCMTI-V (Cai et al., 1996), in conjunction with the three-dimensional solution structure of the protein (Liu et al., 1996), led to the conclusion that the side chain of Arg^{50} was hydrogen-bonded to any of the main chain oxygen atoms of residues 45−47. The S^2 value of 0.78 determined for the Arg^{50} N_ϵH in rCMTI-V* in the present study provides evidence for the conserved

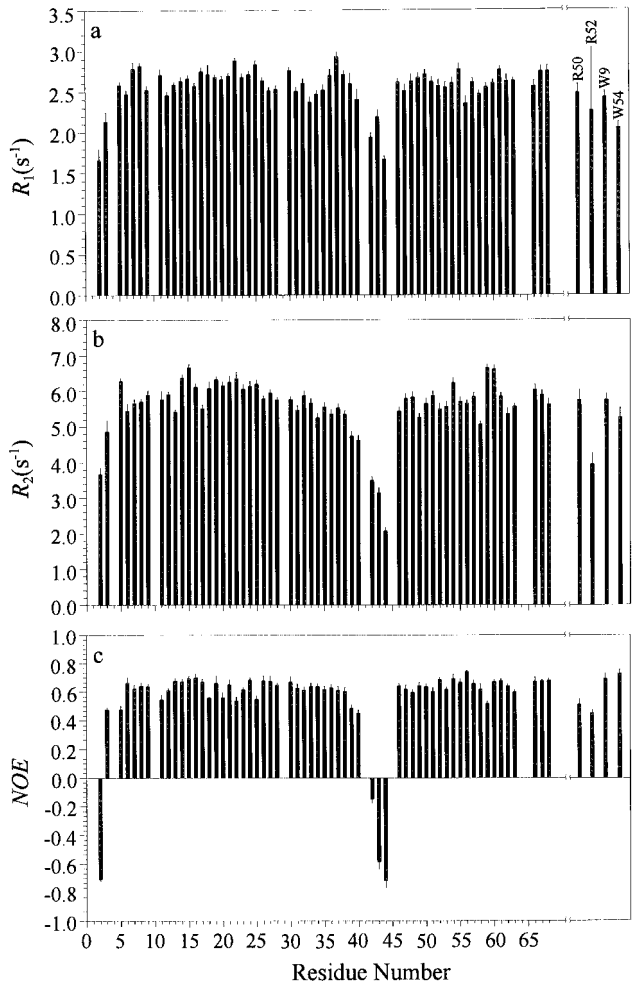

FIGURE 3: Plot of the measured ^{15}N relaxation parameters as a function of amino acid residue number for rCMTI-V*; data for $N_\epsilon Hs$ of Arg^{50}, Arg^{52}, Trp^9, and Trp^{54} are also presented: (a) spin-lattice relaxation rate constants (R_1), (b) spin−spin relaxation rate constants (R_2), (c) $\{^1H\}-^{15}N$ steady-state NOE enhancements. Error bars represent standard deviations calculated from the optimization of eqs 1−3 in the text. Data were not obtained for the N-terminal Gly, Ser^1, Asp^{45}, and six Pro residues.

hydrogen bond to the second binding loop fragment (residues 45−48). From the S^2 values shown by residues 45−48 (Table 2), it may be inferred that the hydrogen bond acceptor of Arg^{50} is most likely the main chain oxygen atom of Asp^{45}; if either Phe^{46} or Arg^{47} were the case, one would expect the NH group(s) of Phe^{46} or Phe^{46} and Arg^{47} to exhibit much lower S^2 values, values similar to those of free N-terminal residues.

The S^2 value of the Arg^{52} $N_\epsilon H$ is lower than that of Arg^{50} (Table 3). That difference appears greater in rCMTI-V*, thus suggesting that the Arg^{52} hydrogen bond is probably weakened in the clipped inhibitor. This explanation is consistent with the increased mobility of residues 39−44 (Table 2) in the first binding loop fragment. The solution structure of rCMTI-V (Liu et al., 1996) reveals that the Arg^{52} side chain can be hydrogen-bonded to the main chain oxygen atom of Val^{42} or Thr^{43} or the side chain oxygen atom of Thr^{43}. The structural details of CMTI-V* (Cai et al., 1995b), together with the order parameters determined for residues 39−44 in rCMTI-V* (Table 2), provide clues as to the identity of the hydrogen bond acceptor of the Arg^{52} side chain. The average RMSDs associated with the backbone atoms of residues 39−44 and 45−48 in the family of 20 NMR solution structures determined for CMTI-V* are 4.3 ± 2.1 and 2.5 ± 1.8 Å, respectively (Cai et al., 1995b). Similarly, the RMSDs between the refined average NMR solution structures of CMTI-V and CMTI-V* (Cai et al., 1995b) indicate a significantly larger displacement of 3.8−16.7 Å for the first fragment (39−44), as compared to 1.3−5.9 Å for the second fragment (46−49). These observations are consistent with the dynamical results that find the first fragment (39−44) flexible and the second (46−48) rigid (Table 2). This also leads to the inference that the main chain oxygen atom of Val^{42} or Thr^{43} may be ruled out as the hydrogen bond partner of the Arg^{52} side chain; it seems unlikely that a hydrogen bond could be conserved between a main chain atom in the binding loop fragment (39−44) that exhibits a large displacement and the $N_\epsilon H$ of Arg^{52} in the protein rigid core that shows one of the smallest displacements, as compared to the intact protein (Cai et al., 1995b). Furthermore, the order parameters determined for residues 39−44 (Table 2) suggest that the hydrogen bond donor is probably the side chain oxygen of Thr^{43}. Significant gains in the mobility of peptide NHs of Thr^{40}, Val^{42}, and Thr^{43} would not be expected, if the main chain oxygen atom of Val^{42} or Thr^{43} were the hydrogen bond acceptor of the Arg^{52} side chain.

Side Chain Dynamics of Trp^9 and Trp^{54}. Both tryptophan rings remain as rigid in rCMTI-V* as they are in the intact protein, as revealed by their order parameters of 0.84 and 0.71, respectively (Table 3). The Trp^9 side chain in rCMTI-V is located in the core of the protein and is stabilized through hydrogen bonding and hydrophobic interactions with surrounding groups: Lys^6, Leu^{12}, Val^{13}, Asn^{22}, Ile^{23}, Ile^{24}, Gln^{27}, Asn^{28}, Pro^{64}, Pro^{65}, Arg^{66}, and Ile^{67} (Liu et al., 1996; Cai et al., 1996). The solution structure of CMTI-V* (Cai et al., 1995b) shows higher RMSDs and differences in NOE patterns for Trp^9. Clearly, the implicated structural changes do not affect the motion of this residue on a time scale faster than the overall tumbling rate of the protein molecule. Similarly, the Trp^{54} ring dynamics is not perturbed between the intact and hydrolyzed forms of the inhibitor. Presumably, the large number of hydrophobic interactions that exists between Trp^{54} and the binding loop residues (Leu^{36}, Glu^{37}, Glu^{38}, Thr^{40}, and Val^{42}) in rCMTI-V (Liu et al., 1996; Cai et al., 1996) is conserved in rCMTI-V*.

Binding Loop Flexibility and Function. The present dynamical results shed light on the relation between flexibility and function in CMTI-V; our earlier results on the trypsin-catalyzed hydrolysis of R50 and R52 mutants of rCMTI-V have indicated that the R50 mutants exhibited enhanced vulnerability to fragmentation than the R52 versions (Cai et al., 1996). The difference was suggested to be due to increased binding loop flexibility in the R50 mutants, on the basis of RP-HPLC retention times. The internal mobility characterized for rCMTI-V* clearly shows retention of anchoring of the second binding loop fragment by the Arg^{50} side chain; very likely, that rigid conformation helps prevent enzyme attacks at other sites of the inhibitor. Removal of the Arg^{52} anchor to the first fragment results in further degradation of the clipped inhibitor, but it occurs at a much slower rate, on a time scale of days as compared to hours in the case of R50 mutants (Cai et al., 1996). The increased flexibility of rCMTI-V* is also reflected in the gain in standard entropy of the system (Cai et al., 1996). Apparently, the flexible structure of rCMTI-V* results in a

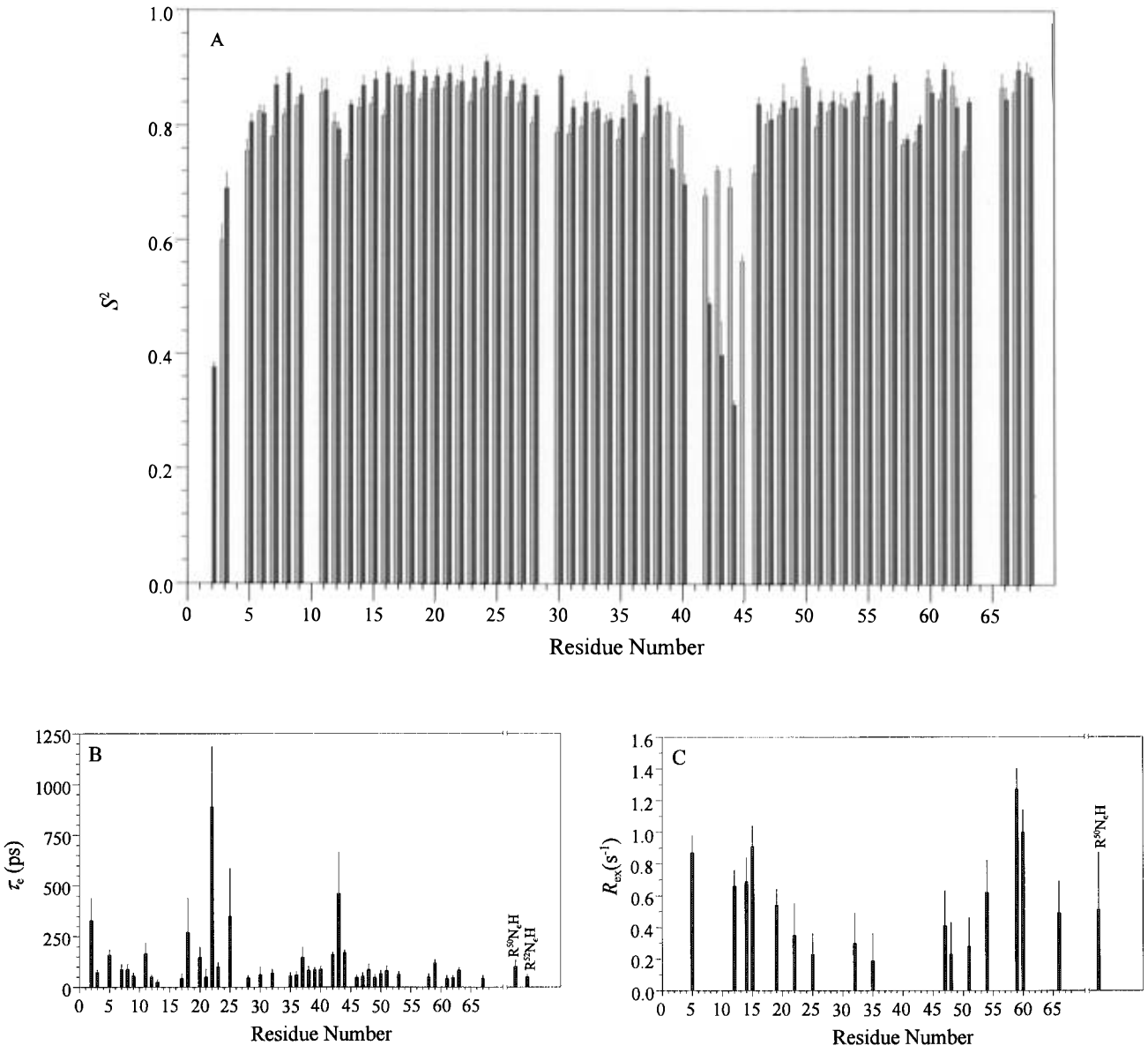

FIGURE 4: Plot of the model-free parameters as a function of amino acid residue number for rCMTI-V*; also shown are data for N_ϵHs of Arg^{50}, Arg^{52}, Trp^{9}, and Trp^{54}. (A) Generalized order parameters (S^2) as compared with those of the intact inhibitor. Solid bars represent S^2 values of rCMTI-V*, and hatched bars represent S^2 values of rCMTI-V, taken from Liu et al. (1996); (B) Effective correlation time for internal motions (τ_e) in picosecond; (C) chemical exchange term (R_{ex}) in hertz.

less-ordered water structure around the protein binding loop region. The hydrolysis equilibrium is found to lie in favor of the clipped inhibitor ($K_{hyd} \approx 11$; Cai et al., 1996). On the basis of the results obtained so far, it seems reasonable to conclude that one way of controlling the equilibrium between rCMTI-V and rCMTI-V* in favor of the intact form would be to make the binding loop segments less flexible in the modified form. Such an approach is desirable in view of the fact that the modified form loses significantly its inhibitory activity toward both trypsin and factor XIIa (Cai et al., 1995b).

Comparison between rCMTI-V and the Noncovalent Complex of Chymotrypsin Inhibitor-2 [CI-2(20−59)·(60−83)].* The overall correlation time, τ_m, for the 64-residue truncated form of CI-2 noncovalent complex has been determined to be 4.42 ns, whereas it is 4.77 ns for the native protein (Shaw et al., 1995). The value determined in the present study is 3.93 ns for rCMTI-V*; a value of 4.43 ns was arrived at for rCMTI-V earlier (Liu et al., 1996). The increase in tumbling rate observed for the nicked inhibitor may be due to differences in interactions between the solvent and the protein in the two forms, as reflected in a positive entropy change observed for the hydrolysis equilibrium (Cai et al., 1995b). A similar change in the overall tumbling time was observed for rCMTI-V at pH 5.0 and 2.5, and it was attributed to differences in solvation as a result of neutralization of carboxylate groups (Cai et al., 1996). The average order parameters for CI-2 and CI-2(20−59)·(60−83) are 0.87 and 0.90, respectively (Shaw et al., 1995), whereas they are 0.83 and 0.85 for rCMTI-V and rCMTI-V*, respectively. In the case of CI-2, all the residues making up the binding loop show increased mobility upon breaking the reactive-site peptide bond between residues 59 and 60; the first half of the loop (residues 53−59) becomes more mobile than the second half (residues 60−64). In the case of rCMTI-V*, the first binding loop segment (39−44) becomes more mobile, whereas the second part (residues 46−49) remains as rigid as the backbone of the structured regions (Table 2).

Table 1: Comparison of Mean Order Parameters of Secondary Structure Elements in rCMTI-V and rCMTI-V*

secondary structure	sequence	number of residues[a]	$\langle S^2 \rangle^b$ rCMTI-V[c]	$\langle S^2 \rangle^b$ rCMTI-V*
α	18−28	11	0.85 ± 0.02	0.88 ± 0.02
β1	7−9	3	0.81 ± 0.03	0.87 ± 0.02
β2	32−38	7	0.81 ± 0.03	0.84 ± 0.03
β3	51−56	6	0.83 ± 0.02	0.85 ± 0.02
β4	54−56	3	0.83 ± 0.02	0.87 ± 0.02
β5	60−62	3	0.87 ± 0.01	0.86 ± 0.03
β6	65−67	2	0.86 ± 0.01	0.87 ± 0.04
T(I)	12−15	4	0.79 ± 0.03	0.85 ± 0.04
$T(II_a)$	28−31	3	0.79 ± 0.01	0.86 ± 0.03
$T(II_b)$	47−50	4	0.82 ± 0.01[d]	0.84 ± 0.02
T(III)	57−60	4	0.81 ± 0.05	0.83 ± 0.05
Binding Loop Segments				
	39−44	5[e]	0.74 ± 0.07	0.51 ± 0.19
	46−48	3	0.78 ± 0.05	0.83 ± 0.02
N-Terminal Region				
	3−6	3[e]	0.73 ± 0.12	0.77 ± 0.07

[a] Number of residues in each secondary structural element for which relaxation data were obtained. [b] Average order parameter, calculated from Table S-2 (in supporting information). [c] Data for rCMTI-V were obtained from previously published results (Liu et al., 1996). [d] Average of three out of four residues. Residue 50 was excluded in the average (Liu et al., 1996). [e] No data available for Pro^{41}.

Table 2: Comparison of Order Parameters of Binding Loop Residues in rCMTI-V and rCMTI-V*

residue number	S^2 rCMTI-V[a]	S^2 rCMTI-V*
Leu^{36}	0.86 ± 0.03	0.84 ± 0.02
Glu^{37}	0.78 ± 0.01	0.89 ± 0.01
Glu^{38}	0.82 ± 0.01	0.84 ± 0.01
Gly^{39}	0.82 ± 0.02	0.73 ± 0.02
Thr^{40}	0.80 ± 0.01	0.70 ± 0.02
Val^{42}	0.68 ± 0.01	0.49 ± 0.01
Thr^{43}	0.72 ± 0.01	0.40 ± 0.06
Lys^{44}	0.69 ± 0.03	0.31 ± 0.01
Asp^{45}	0.56 ± 0.01	na[b]
Phe^{46}	0.72 ± 0.01	0.84 ± 0.01
Arg^{47}	0.80 ± 0.02	0.81 ± 0.03
Cys^{48}	0.82 ± 0.01	0.84 ± 0.03

[a] Data taken from Liu et al, 1996. [b] Data not available due to the cleavage of the reactive-site (Lys^{44}−Asp^{45}) peptide bond.

Table 3: Comparison of Order Parameters of Arginine and Tryptophan N_ϵHs in rCMTI-V and rCMTI-V*

residue number	S^2 rCMTI-V[a]	S^2 rCMTI-V*
Arg^{50}	0.73 ± 0.01	0.78 ± 0.03
Arg^{52}	0.63 ± 0.01	0.59 ± 0.04
Trp^{9}	0.79 ± 0.01	0.84 ± 0.02
Trp^{54}	0.73 ± 0.01	0.71 ± 0.02

[a] Data taken from Cai et al. (1996).

These results suggest that Arg^{50} probably stabilizes the binding loop fragment more in rCMTI-V* than its counterpart in the CI-2 noncovalent complex. Furthermore, the three-dimensional solution structure determined for CMTI-V* (Cai et al., 1995b) reveals that the two binding loop fragments move away from each other, which is probably assisted by the presence of the unique Cys^3−Cys^{48} disulfide bridge. In the case of the noncovalent complex of CI-2, the rigidity of the second binding loop fragment has been interpreted as an indication of conservation of its position in space with respect to the scaffold region in the intact protein (Shaw et al., 1995). Similar τ_e values were obtained for both proteins. However, no interpretation of these values is attempted in this study.

CONCLUSIONS

Hydrolysis of the reactive site (Lys^{44}-Asp^{45} peptide bond) in rCMTI-V does not affect the backbone dynamics of the structured, scaffold region of the inhibitor. The first fragment of the binding loop (residues 39−44) shows increased internal mobility, whereas the second fragment (46−48) remains as rigid as most of the protein backbone. The Arg^{52} hydrogen bond to the first binding loop segment is thus weaker than the Arg^{50} hydrogen bond to the second fragment. This is supported by the order parameters determined for the N_ϵHs of Arg^{50} and Arg^{52}. The main chain oxygen atom of Asp^{45} and the side chain oxygen atom of Thr^{43} appear to be the hydrogen bond acceptors of the side chains of Arg^{50} and Arg^{52}, respectively. The RMSDs associated with the two binding loop fragments of CMTI-V* in the family of NMR solution structures are found to be consistent with the findings of the internal dynamics study.

SUPPORTING INFORMATION AVAILABLE

Two figures showing the ^{15}N chemical shift differences between rCMTI-V and rCMTI-V* and the ^1H chemical shift differences between rCMTI-V* and CMTI-V* and two tables containing experimental R_1, R_2, and NOE measurements and computed model-free parameters (S^2, τ_e, and R_{ex}) of rCMTI-V* (8 pages). Ordering information is given on any current masthead page.

REFERENCES

Basus, V. J. (1989) *Methods Enzymol. 177*, 132−149.

Bode, W., Epp, O., Huber, R., Laskowski, M., Jr., & Ardelt, W. (1985) *Eur. J. Biochem. 147*, 387−395.

Bode, W., Greyling, H. J., Huber, R., Otlewski, J., & Wilusz, T. (1989) *FEBS Lett. 242*, 285−292.

Bodenhausen, G., & Ruben, D. J. (1980) *Chem. Phys. Lett. 69*, 185−189.

Cai, M., Gong, Y., Kao, J. L.-F., & Krishnamoorthi, R. (1995a) *Biochemistry 34*, 5201−5211.

Cai, M., Gong, Y., Prakash, O., & Krishnamoorthi, R. (1995b) *Biochemistry 34*, 12087−12094.

Cai, M., Liu, J., Gong, Y., & Krishnamoorthi, R. (1995c) *J. Magn. Reson., Ser. B 107*, 172−178.

Cai, M., Huang, Y., Prakash, O., Wen, L., Han, S. K., & Krishnamoorthi, R. (1995d) *J. Magn. Reson., Ser. B 108*, 189−191.

Cai, M., Huang, Y., Prakash, O., Wen, L., Dunkelbarger, S. P., Huang, J.-K., Liu, J., & Krishnamoorthi, R. (1996) *Biochemistry 35*, 4784−4794.

Cavanagh, J., Palmer, A. G., Wright, P. E., & Rance, M. (1991) *J. Magn. Reson. 91*, 429−436.

Clore, G. M., Appella, E., Yamada, M., Matsushima, K., & Gronenborn, A. M. (1990a) *Biochemistry 29*, 1689−1696.

Clore, G. M., Szabo, A., Bax, A., Kay, L. E., Driscoll, P. C., & Gronenborn, A. M. (1990b) *J. Am. Chem. Soc. 112*, 4989−4991.

Hipler, K., Priestle, J. P., Rahuel, J., & Grutter, M. G. (1992) *FEBS Lett. 309*, 139−145.

Hojima, Y., Pierce, J. V., & Pisano, J. J. (1982) *Biochemistry 21*, 3741−3746.

Huang, K., Lu, W., Anderson, S., Laskowski, M., Jr., & James, M. N. G. (1995) *Protein Sci. 4*, 1985−1997.

Hyberts, S. G., Goldberg, M. S., Havel, T. F., & Wagner, G. (1992) *Protein Sci. 1*, 736−751.

Karplus, M. (1986) *Methods Enzymol. 131*, 283−307.

Karplus, M., & McCammon, J. A. (1983) *Annu. Rev. Biochem. 52*, 263−300.
Kay, L. E., Torchia, D. A., & Bax, A. (1989b) *Biochemistry 28*, 8972−8979.
Krezel, A. M., Darba, P., Robertson, A. D., Fejzo, J., Macura, S., & Markley, J. L. (1994) *J. Mol. Biol. 242*, 203−214.
Krishnamoorthi, R., Gong, Y., & Richardson, M. (1990) *FEBS Lett. 273*, 163−167.
Krishnamoorthi, R., Gong, Y., Linc, C.-L. S., & VanderVelde, D. (1992a) *Biochemistry 31*, 898−904.
Krishnamoorthi, R., Lin, C.-L. S., & VanderVelde, D. (1992b) *Biochemistry 31*, 4965−4969.
Laskowski, M., Jr., & Kato, I. (1980) *Annu. Rev. Biochem. 49*, 593−626.
Lipari, G., & Szabo, A. (1982a) *J. Am. Chem. Soc. 104*, 4546−4559.
Lipari, G., & Szabo, A. (1982b) *J. Am. Chem. Soc. 104*, 4559−4570.
Liu, J., Prakash, O., Cai, M., Gong, Y., Huang, Y., Wen, L., Wen, J. J., Huang, J. -K., & Krishnamoorthi, R. (1996) *Biochemistry 35*, 1516−1524.
Live, D. H., Davis, D. G., Agosta, W. C., & Cowburn, D. (1984) *J. Am. Chem. Soc. 106*, 1939−1941.
Ludvigsen, S., Shen, H., Kjaer, M., Madsen, J. C., & Poulsen, F. M. (1991) *J. Mol. Biol.* 222, 621−635.
Marion, D., Ikura, M., & Bax, A. (1989) *J. Magn. Reson. 84*, 425−430.
McPhalen, C. A., & James, M. N. G. (1987) *Biochemistry 26*, 261−269.
Meiboom, S., & Gill, D. (1958) *Rev. Sci. Instrum. 29*, 688−691.
Musil, D., Bode, W., Huber, R., Laskowski, M., Jr., Lin, T.-Y., & Ardelt, W. (1991) *J. Mol. Biol. 220*, 739−755.
Noggle, J. H., & Shirmer, R. E. (1971) *The Nuclear Overhauser Effect: Chemical Applications*, Academic Press, New York.
Palmer, A. G., Cavanagh, J., Write, P. E., & Rance, M. (1991) *J. Magn. Reson. 93*, 151−170.
Papamokos, E., Weber, E., Bode, W., Empie, H. W., Kato, I., & Laskowski, M., Jr. (1982) *J. Mol. Biol. 158*, 515−537.
Peng, J. W., & Wagner, G. (1994) *Methods Enzymol. 239*, 563−596.
Shaw, G. L., Davis, B., Keeler, J., & Fersht, A. (1995) *Biochemistry 34*, 2225−2233.
Skelton, N. J., Palmer, A. G., Akke, M., Kördel, J., Rance, M., & Chazin W. (1993) *J. Magn. Reson., Ser. B 102*, 253−264.
Vold, R. L., Waugh, J. S., Klein, M. P., & Phelps, D. E. (1968) *J. Chem. Phys. 48*, 3831−3832.
Walkenhorst, W. F., Krezel, A. M., Rhyu, G. I., & Markley, J. L. (1994) *J. Mol. Biol. 242*, 215−230.
Wen, L., Kim, S., Tinn, T. T., Huang, J., Krishnamoorthi, R., Gong, Y., Lwin, Y. N., & Kyin, S. (1993) *Protein Expression Purif. 4*, 215−222.
Wynn, R., & Laskowski, M., Jr. (1990) *Biochem. Biophys. Res. Commun. 166*, 1406−1410.

BI9609329